Fault-tolerant Hahn-Ramsey interferometry with pulse sequences of alternating detuning

Nikolay V. Vitanov,[1] Timm F. Gloger,[2] Peter Kaufmann,[2] Delia Kaufmann,[2] Thomas Collath,[2] M. Tanveer Baig,[2] Michael Johanning,[2] and Christof Wunderlich[2]

[1]*Department of Physics, St Kliment Ohridski University of Sofia, 5 James Bourchier Boulevard, 1164 Sofia, Bulgaria*

[2]*Department Physik, Naturwissenschaftlich-Technische Fakultät, Universität Siegen, 57068 Siegen, Germany*

(Received 29 August 2014; published 23 March 2015)

A scheme for efficient correction of driving-field frequency drifts in Ramsey interferometry is proposed. The two off-resonant $\pi/2$ pulses of duration T used in the traditional Ramsey setup are supplemented with an additional pulse of duration $2T$ (approximate π pulse), which is applied midway between the Ramsey pulses and has a detuning of opposite sign to theirs. This scheme, which resembles a Hahn's spin-echo pulse embedded into the Ramsey setup, corrects small-to-moderate random errors in the detuning of the driving field. This allows the observation of Ramsey fringes of high contrast even with a noisy driving field or in inhomogeneously broadened atomic ensembles. The contrast is further improved by replacing the refocusing $2T$ pulse by a composite π pulse. We demonstrate the validity of the concept by comparing experimental results from usual Ramsey measurements with Hahn-Ramsey measurements. These experimental results are obtained from microwave-optical double-resonance spectroscopy on $^{171}Yb^{+}$ ions in a segmented linear Paul trap. In the same way, we verify qualitatively the predicted advantage from using a composite π pulse for refocusing.

DOI: 10.1103/PhysRevA.91.033406 PACS number(s): 42.50.Md, 32.80.Qk, 32.70.Jz, 06.30.Ft

I. INTRODUCTION

Ramsey interferometry is nowadays a textbook technique in experimental quantum physics [1–6]. The traditional Ramsey setup involves the interaction of a two-state quantum system with two separated oscillating external fields, in either space [1] or time [3]. The fields are intentionally detuned from resonance with the Bohr transition frequency of the quantum system by a suitably chosen detuning Δ, and the durations of the two driving pulses are selected to produce the effect of $\pi/2$ pulses. Ramsey fringes emerge when the transition probability is plotted versus the detuning Δ or the pulse separation τ. Alternatively, Ramsey fringes can be produced when varying the relative phase between the two $\pi/2$ pulses [2]; the latter feature makes it possible to use Ramsey interferometry for measuring phases [7,8]. It has also been recognized that an enhanced sensitivity can be achieved by using multiple control pulses [4,9].

While its primary application is in high-precision metrology, e.g., in atomic clocks [10], Ramsey spectroscopy is a very convenient tool in other branches of quantum physics too. One such application, which is of primary interest here, is the detection and characterization of quantum coherence and the measurement of decoherence times [11–14]. Inasmuch as Ramsey fringes are an interference pattern, which depends strongly on the coherence of the quantum system, the fringes are sensitive to any decoherence process during the Ramsey interaction and are therefore a convenient tool for probing and characterizing coherence.

Because the Ramsey fringes depend strongly on the detuning, they are sensitive to any systematic shifts, e.g., driving-field-induced Stark shifts [10,15], or fluctuations in this detuning [14]. Unless the experimental apparatus is frequency stabilized to a very high accuracy, frequency fluctuations in the course of collecting the data may easily spoil the contrast of the fringes [14].

In this paper, we propose and demonstrate a modification of the Ramsey setup by adding an approximate π pulse between the two Ramsey $\pi/2$ pulses, in a manner reminiscent of Hahn's spin-echo technique [16]. In contrast to the earlier use of a spin-echo π pulse in Ramsey interferometry [8,13], which eliminates the effect of the detuning (to first order), here we use an off-resonant approximate π pulse of opposite detuning to that of the Ramsey $\pi/2$ pulses. This method, which we refer to as fault-tolerant Hahn-Ramsey interferometry, preserves the dependence of the fringes on the detuning (which defines the fringe frequency), but it eliminates small-to-moderate fluctuations in this detuning, thereby greatly enhancing the fringe contrast in the presence of detuning drifts. Provided the Rabi frequency of the driving field is sufficiently larger than the detuning (a factor of 5 or more) the Ramsey fringes are essentially unaffected by the detuning fluctuations. We derive explicit analytic formulas for these fault-tolerant Hahn-Ramsey fringes and the corrections to them due to detuning fluctuations. Then we proceed with an experimental verification of the Hahn-Ramsey technique with $^{171}Yb^{+}$ ions trapped in a segmented linear Paul trap.

This reduced sensitivity of the Ramsey fringes to field variations is opposite to the use of Ramsey interferometry to measure small light shifts or phases when enhanced sensitivity is required, e.g., in quantum metrology [7]. Therefore, the present paper treats specifically the use of Ramsey interferometry for detection and characterization of quantum coherence over long storage times when the stability of the control fields is of crucial importance. It gives a prescription for increasing the resolution of the Ramsey fringes in the presence of driving-field frequency drifts during the course of measurement.

This paper is organized as follows. Section II reviews the standard Ramsey setup and its limitations. Section III introduces the fault-tolerant Hahn-Ramsey interferometry and presents its theory. Section IV describes the experimental setup for the realization of the proposed technique, and Sec. V presents the experimental results. Finally, Sec. VI discusses the relation of the fault-tolerant Hahn-Ramsey technique to similar techniques, and Sec. VII summarizes the conclusions.

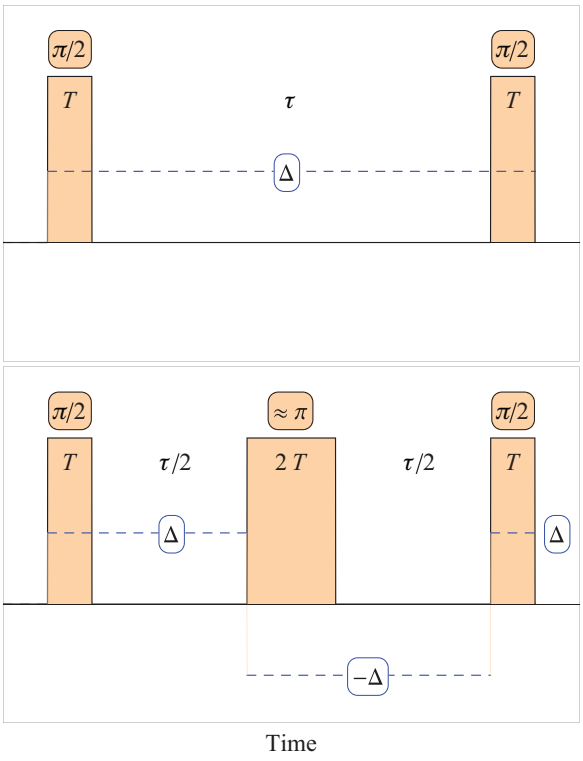

FIG. 1. (Color online) Pulses in the traditional Ramsey scheme (top, two $\pi/2$ pulses of duration T) and the fault-tolerant Hahn-Ramsey scheme proposed here (bottom, three pulses of durations T, $2T$, and T). The detuning Δ is kept constant in the Ramsey scheme, while in the fault-tolerant Hahn-Ramsey scheme, its sign is flipped with the application of the intermediate $2T$ pulse, and then restored to its original value in the last $\pi/2$ pulse.

II. STANDARD RAMSEY INTERFEROMETRY

A. Basic theory

The classical Ramsey interferometer consists of a pair of $\pi/2$ pulses of duration T producing qubit rotation $R(T)$, separated by free evolution $F(\tau)$ for time τ, as illustrated in Fig. 1 (top). Here we shall first summarize the theory of ideal Ramsey fringes and then analyze how errors in the Rabi frequency and the detuning affect them.

We work in the rotating-wave picture [17] in which the rapidly rotating [at the transition frequency $\omega_0 = \omega_2 - \omega_1 = (E_2 - E_1)/\hbar$] probability amplitudes of the two states $a_1(t)$ and $a_2(t)$ are replaced by the slowly varying (at the field-atom detuning Δ) amplitudes $c_1(t)$ and $c_2(t)$. The Hamiltonian for each pulse in the rotating-wave approximation reads [17]

$$\mathbf{H} = \frac{\hbar}{2}\begin{bmatrix} -\Delta & \Omega e^{i\phi} \\ \Omega e^{-i\phi} & \Delta \end{bmatrix}. \tag{1}$$

The detuning from resonance, Δ, which is assumed positive without loss of generality, controls the period of the Ramsey fringes; hence we shall use Δ as the unit for frequency and $1/\Delta$ as the unit for time. The coupling between the two states is quantified by the Rabi frequency Ω, which is assumed positive, and it may have a phase ϕ, as is the case with composite pulses [18]. We consider for simplicity rectangular pulses of width T and Rabi frequency Ω, as in most applications of the Ramsey method. Each of the two rectangular pulses produces the propagator $\mathbf{R}_\phi(T) = \exp(-i\mathbf{H}T/\hbar)$; explicitly,

$$\mathbf{R}_\phi(T) = \begin{bmatrix} \cos\frac{1}{2}A + i\frac{\Delta}{\widetilde{\Omega}}\sin\frac{1}{2}A & -ie^{i\phi}\frac{\Omega}{\widetilde{\Omega}}\sin\frac{1}{2}A \\ -ie^{-i\phi}\frac{\Omega}{\widetilde{\Omega}}\sin\frac{1}{2}A & \cos\frac{1}{2}A - i\frac{\Delta}{\widetilde{\Omega}}\sin\frac{1}{2}A \end{bmatrix}, \tag{2}$$

where $\widetilde{\Omega} = \sqrt{\Omega^2 + \Delta^2}$ and $A = \widetilde{\Omega}T$ is the generalized pulse area. The transition probability is given by the Rabi formula

$$p = \frac{\Omega^2}{\Omega^2 + \Delta^2}\sin^2\left(\frac{T}{2}\sqrt{\Omega^2 + \Delta^2}\right). \tag{3}$$

On exact resonance one would have a pulse area $\Omega T = \pi/2$ for each Ramsey pulse; however, for nonzero detuning this value increases. An effective half-π pulse, i.e., one that produces transition probability $p = \frac{1}{2}$, takes place for the pulse duration

$$T = \frac{2}{\sqrt{\Omega^2 + \Delta^2}}\arcsin\frac{\sqrt{\Omega^2 + \Delta^2}}{\Omega\sqrt{2}}, \tag{4}$$

which we assume hereafter. Obviously, such a probability can be produced only if $\Delta \leqq \Omega$. Although this latter condition suffices for most of the results below to be valid, we shall rather assume the stronger condition $\Delta \ll \Omega$, which is usually fulfilled in Ramsey spectroscopy.

The free evolution of the two-state system is described by the propagator

$$\mathbf{F}(\tau) = \begin{bmatrix} e^{i\Delta\tau/2} & 0 \\ 0 & e^{-i\Delta\tau/2} \end{bmatrix}. \tag{5}$$

The overall propagator of the standard Ramsey scheme is

$$\mathbf{U} = \mathbf{R}_\phi(T)\mathbf{F}(\tau)\mathbf{R}_0(T), \tag{6}$$

where ϕ is the relative phase between the two pulses. Because it is only the relative phase between the two Ramsey pulses that matters, we have set the phase of the first pulse to zero.

B. Errorless Ramsey fringes

The exact formula for the ideal Ramsey fringes reads

$$P = |U_{12}|^2 = \cos^2\left(\frac{\Delta\tau}{2} + \chi + \frac{\phi}{2}\right), \tag{7}$$

where

$$\chi = \arcsin\frac{\Delta}{\Omega}. \tag{8}$$

If $\Delta \ll \Omega$ then $\chi \ll 1$. Note that the phase shift χ depends on Ω and Δ only and does not change when the pulse delay τ is varied. As the main concern here is the behavior of the Ramsey fringes versus the pulse delay τ, we will set the relative phase ϕ to zero: $\phi = 0$.

The Ramsey fringes in the errorless case are depicted in Fig. 2 by a solid curve. The fringes follow a sinusoid curve versus the pulse delay τ with a frequency Δ and are shifted by a phase χ. In the limit $\tau \to 0$, the two Ramsey pulses merge into a single pulse. However, because these are off-resonant effective $\pi/2$ pulses, rather than resonant $\pi/2$ pulses, their merger does not produce an effective π pulse (and hence $P = 1$) but rather the probability $P = \cos^2\chi = 1 - \Delta^2/\Omega^2 < 1$. This feature complies with the fact

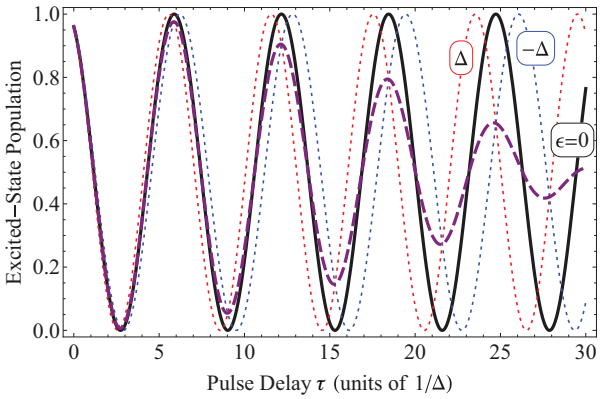

FIG. 2. (Color online) Ramsey signal produced by a standard two-pulse Ramsey setup. Full curve, no error, $\epsilon = 0$; dotted curves, signals for detunings Δ and $-\Delta$ and error $\epsilon = 0.05\Delta$; dashed curve, average of the dotted curves. The Rabi frequency is $\Omega = 5\Delta$.

that a rectangular pulse of constant detuning cannot produce complete population transfer. (Complete population transfer can still happen for a suitably chosen relative phase between the two pulses: $\phi = -2\chi$. This fact does not contradict the preceding statement because a nonzero phase step corresponds to a δ-function jump in the detuning.)

C. Ramsey fringes in the presence of detuning and amplitude errors

In a typical experiment, each point of the Ramsey fringes is an average of a large number of data points, and taking the full scan may exceed the time scale during which the driving-field frequency or/and amplitude stays fixed. In order to estimate the effect of errors in the detuning and the Rabi frequency we set $\Delta \to \Delta + \epsilon$ and $\Omega \to \Omega + \alpha$. A simple calculation in the limit $|\epsilon| \ll \Delta$ and $|\alpha| \ll \Omega$ gives the following estimate (to the lowest orders of ϵ and α):

$$P \approx \cos^2\left(\frac{\Delta\tau}{2} + \chi + \frac{\epsilon\tau}{2} - \frac{\Delta\alpha}{\Omega\sqrt{\Omega^2 - \Delta^2}}\right). \quad (9)$$

The α term is negligibly small due to the condition $\Omega \gg \Delta$ and it leads to only a small shift in the fringes. The ϵ term, however, may become very large for large pulse delay τ (which is the case in Ramsey spectroscopy) and it changes the Ramsey fringes considerably. The Ramsey fringes for nonzero detuning error ϵ are depicted in Fig. 2 by two dashed curves (for detunings Δ and $-\Delta$). Obviously, superposing measurements for different ϵ will make the Ramsey fringes dephase rapidly and will result in much lower contrast. Therefore, hereafter we neglect the Rabi frequency error α and we shall discuss two strategies to dynamically reduce the effect of detuning errors.

The main problem is that the detuning error acts continuously, during the Ramsey pulses as well as during the free evolution of the system. This makes the current problem different from, and more difficult than, a recent proposal [15] and an experiment [10], which compensate the dynamical Stark shift induced by the driving pulses themselves; this shift is present only during the driving pulses.

We assume below that variations in the detuning do not take place during the measurement of each data point but only from one measurement to another. In other words, the faulty detuning $\Delta + \epsilon$ stays constant during each measurement but the error ϵ may be different for different measurements. Our objective is to find strategies for which the Ramsey fringes are locked to the detuning Δ and do not depend on the error ϵ within a certain range.

D. Adding two Ramsey signals of opposite detunings

An intuitive approach to reduce the effect of detuning fluctuations in the standard Ramsey scheme is to add two signals, one for detuning Δ and another for detuning $-\Delta$ [10]. It is essential that the frequency drift ϵ adds up to the detuning in the same manner, $\Delta \to \Delta + \epsilon$ and $-\Delta \to -\Delta + \epsilon$, regardless of the sign of the detuning. This makes it possible to discriminate ϵ from Δ. Figure 2 shows the signal derived in this manner (dashed curve). While the phase of the fringes is largely compensated, their amplitude undergoes sinusoidal modulation, which depends on the detuning error ϵ and the pulse delay τ. In the limit of small ϵ one finds the simple estimate

$$P = \tfrac{1}{2}[1 + \cos(\epsilon\tau)\cos(\Delta\tau + 2\chi)]. \quad (10)$$

This simple formula describes very well the combined signal (dashed curve) in Fig. 2. Obviously, this approach can be used only for small detuning error ϵ and pulse delay τ such that $|\epsilon|\tau \ll 1$.

III. FAULT-TOLERANT HAHN-RAMSEY FRINGES

Here we propose to use ideas similar to Hahn's spin-echo rephasing technique [16] in order to reduce the effect of the detuning error on the Ramsey fringes. The two Ramsey $\pi/2$ pulses, each of duration T, are supplemented with a pulse of duration $2T$ applied in the middle between the two pulses, thereby splitting the free-evolution interval of duration τ into two equal half intervals of duration $\tau/2$ each, as shown in Fig. 1 (bottom). The nontrivial detail here is that the error-correcting $2T$ pulse has the opposite detuning $-\Delta$ compared to the two Ramsey pulses. The implication is that the free evolution in the first interval proceeds with a detuning Δ, while the free evolution in the second interval proceeds with a detuning $-\Delta$ [see Fig. 1 (bottom)] as the free-evolution precession frequency is determined by the last pulse acting upon the system. The free evolution with precession frequencies of opposite signs is the primary reason for the cancellation of the detuning error in the Ramsey fringes. In the presence of an error ϵ, the precession frequency in the first interval is $\Delta + \epsilon$, while in the second interval it is $|-\Delta + \epsilon| = \Delta - \epsilon$ (assuming $\Delta > \epsilon$). The different signs of the error ϵ in the two free-evolution intervals lead to the self-correction of this error.

The overall Hahn-Ramsey propagator (acting from right to left) reads

$$\mathbf{R}_{\Delta+\epsilon}(T)\mathbf{F}_{-\Delta+\epsilon}(\tau/2)\mathbf{R}_{-\Delta+\epsilon}(2T)\mathbf{F}_{\Delta+\epsilon}(\tau/2)\mathbf{R}_{\Delta+\epsilon}(T). \quad (11)$$

The exact transition probability can be calculated from here but the expression is too cumbersome to be of practical interest. In the limit of small detuning error ($|\epsilon| \ll \Delta$) the transition

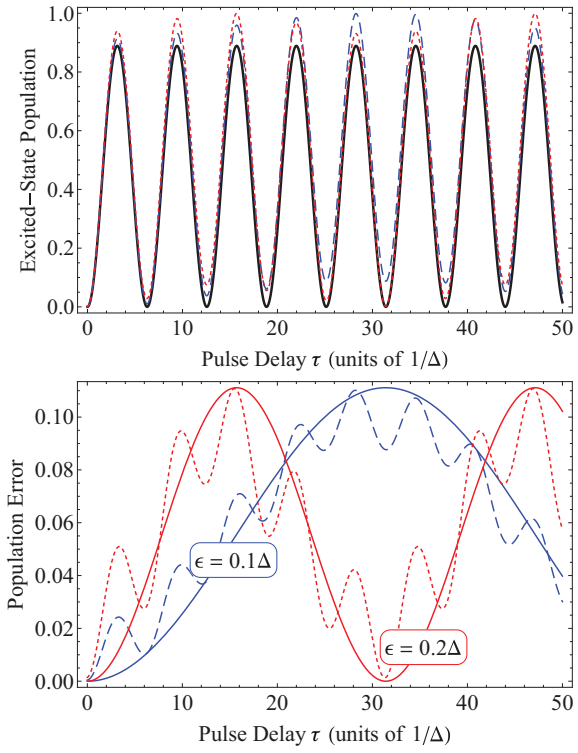

FIG. 3. (Color online) Fault-tolerant Hahn-Ramsey fringes for $\Omega = 3\Delta$. Top frame: Excited-state population. Solid curve, no detuning error, $\epsilon = 0$; dashed curve, $\epsilon = 0.1\Delta$; dotted curve, $\epsilon = 0.2\Delta$. Bottom frame: Deviation from the errorless signal. Solid curves, the second term in the approximation (12); dashed and dotted curves, exact values.

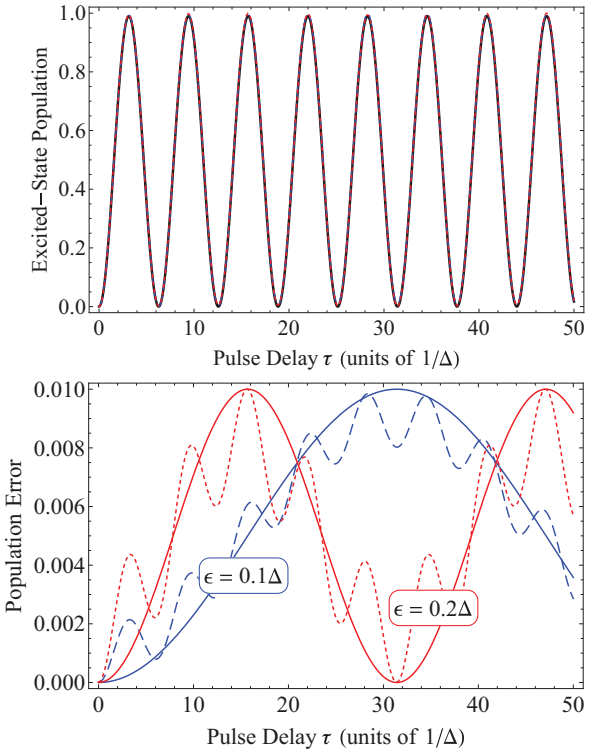

FIG. 4. (Color online) As Fig. 3 but for Rabi frequency $\Omega = 10\Delta$. The error does not exceed 0.01.

probability is approximately given by

$$P \approx \left(1 - \frac{\Delta^2}{\Omega^2}\right) \sin^2 \frac{\Delta\tau}{2} + \frac{\Delta^2}{\Omega^2} \sin^2 \frac{\epsilon\tau}{2}. \qquad (12)$$

Obviously, the leading first term is a sinusoid with a frequency Δ and an amplitude $1 - \Delta^2/\Omega^2$. The second term has the same amplitude Δ^2/Ω^2 as the deviation from 1 of the first term but it oscillates vs τ with a frequency ϵ. Clearly, the fault-tolerant Hahn-Ramsey fringes benefit in terms of contrast by taking a higher ratio Ω^2/Δ^2, which both damps the error term and pushes the fringe amplitude to 1. For $\Omega \gtrsim 5\Delta$, the amplitude is practically equal to 1 and the error term is negligibly small.

Figure 3 shows these features in the Hahn-Ramsey signal for $\Omega/\Delta = 3$. This rather low ratio makes the features clearly visible. The phase of the fringes is not affected by the detuning error, but only their amplitude. The overall modulation of the amplitude of the error is described very well by the error term in Eq. (12). The small-amplitude oscillations of frequency Δ in the error can be described analytically as well but it is barely worth the effort.

Figure 4 shows the Hahn-Ramsey signal for $\Omega/\Delta = 10$, where the presence of the detuning error is barely visible even for the rather high value $\epsilon = 0.2\Delta$. It is easy to verify that even higher errors are easily compensated in this case.

Figure 5 compares the classical Ramsey scheme with the one with two superposed signals for opposite detunings Δ and $-\Delta$, and the fault-tolerant Hahn-Ramsey scheme proposed here in the presence of random detuning errors within a certain interval $(-\epsilon_0, \epsilon_0)$. The classical Ramsey and the superposed-Ramsey fringes decohere very rapidly, even for a small maximum error $\epsilon_0 = 0.05\Delta$. The fault-tolerant Hahn-Ramsey scheme maintains nearly perfect fringe contrast even in the presence of errors as large as 0.3Δ (and even for larger errors, not shown here). Moreover, as the Rabi frequency increases from 3Δ to 5Δ and then 10Δ (the three lower curves) the Hahn-Ramsey signal gradually becomes indistinguishable from the errorless solid curves.

The fault-tolerant Hahn-Ramsey scheme proposed here is imperfect when the ratio Ω/Δ has only moderate values, as seen in Figs. 3 and 5, because even in the errorless limit $\epsilon = 0$ the oscillation amplitude is $1 - \Delta^2/\Omega^2 < 1$, as is evident from Eq. (12). This problem is rooted in the fact that the rephasing pulse of duration $2T$ is not a perfect π pulse, but only an approximate one. This slight drawback can be eliminated, as mentioned above, by using a larger ratio Ω/Δ. If this is not possible, the problem can be alleviated in two ways. (i) First, the rephasing pulse of duration $2T$ and Rabi frequency Ω can be replaced by a pulse of duration T and Rabi frequency 2Ω. It has the same pulse area as before but its effect is closer to that of a π pulse because of the larger Rabi frequency. Indeed, it is easy to verify that the oscillation amplitude now will be $1 - \Delta^2/(4\Omega^2)$, i.e., the deviation from 1 is reduced by a factor of 4. However, one may argue here that simply using a Rabi frequency 2Ω in the original fault-tolerant Hahn-Ramsay setup will achieve the same result, which is certainly true. (ii) Second, one can replace the rephasing pulse of duration $2T$ and Rabi frequency Ω by a composite pulse with the same duration and Rabi frequency. This composite pulse consists of

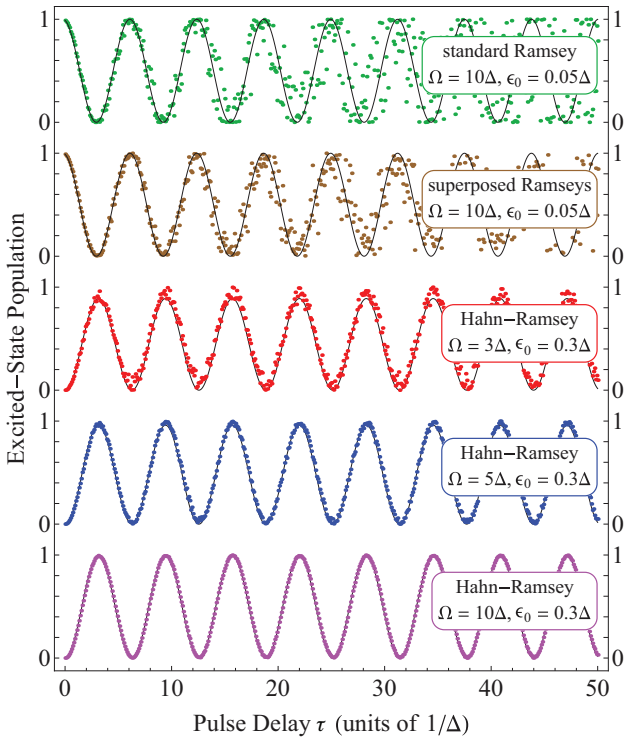

FIG. 5. (Color online) Numerical comparison of the classical Ramsey scheme, the Ramsey scheme with two superposed signals for opposite detunings Δ and $-\Delta$, and the fault-tolerant Hahn-Ramsey scheme proposed here in the presence of random detuning errors. Each point is simulated by taking a random detuning error from the interval $(-\epsilon_0,\epsilon_0)$. The Ramsey fringes (top curve) and the superposed Ramsey fringes (second from top) decohere very fast even though the maximum error is rather small, $\epsilon_0 = 0.05\Delta$. The three lower curves are calculated for much larger maximum detuning errors $\epsilon_0 = 0.3\Delta$, and for three different Rabi frequencies (denoted on each curve). The solid sinusoids refer to the errorless case ($\epsilon_0 = 0$).

two pulses of duration T each, but with a phase $\phi = 2\chi$ of the second pulse relative to the first one. (Because the detuning is $-\Delta$, the composite phase is $\phi = 2\chi$ rather than $\phi = -2\chi$, as it would be the case for detuning Δ.) As is easily seen from Eq. (7) with $\tau = 0$, this composite pulse acts as an ideal π pulse.

Figure 6 compares the fault-tolerant Hahn-Ramsey fringes in the original version T-$2T$-T with the variations (i) and (ii) described above in the case of moderate ratio Ω/Δ when the imperfection of the T-$2T$-T sequence is easily visible. Clearly, using the Rabi frequency 2Ω reduces the errors in the fringes, while using a composite middle pulse produces nearly perfect fringes.

An interesting question is the following: Given that the fault-tolerant Hahn-Ramsey fringes are insensitive to variations in the detuning, how does the quantum system "know" to produce interference fringes with frequency equal to the preselected benchmark detuning Δ? The simple answer to this question lies in the way the duration T of the Ramsey pulses and the duration $2T$ of the Hahn rephasing pulse are selected according to Eq. (4), in which the detuning Δ is explicitly present.

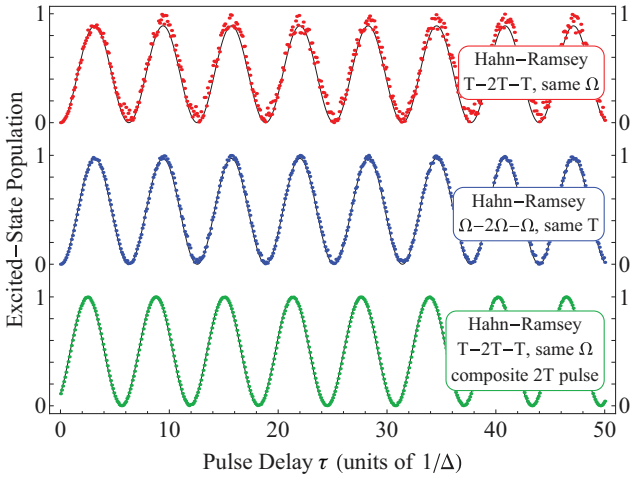

FIG. 6. (Color online) Numerical comparison of the fault-tolerant Hahn-Ramsey scheme proposed here, in the presence of random detuning errors. Each point is simulated by taking a random detuning error from the interval $(-\epsilon_0,\epsilon_0)$, with $\epsilon_0 = 0.3\Delta$. The Rabi frequency is $\Omega = 3\Delta$. Top curve, three pulses of the same Rabi frequency but different durations, T-$2T$-T. Middle curve, three pulses of the same duration T but different Rabi frequencies, Ω-2Ω-Ω. Bottom curve, as the top curve, but with the middle pulse split into two pulses, each of duration T, the second of which is phase shifted by a phase $\phi = 2\chi$. The solid sinusoids refer to the errorless case ($\epsilon_0 = 0$).

IV. EXPERIMENTAL REALIZATION

A. Experimental setup

The experiments were carried out in a segmented three-layer trap made of microstructured, gold coated alumina (as in [19]), modified by a middle layer which provides four independent coils for the generation of magnetic fields and gradients [20]. The trap is mounted to a chip carrier which was processed with thick-film technology to act as a vacuum interface suitable for UHV [20].

All dc voltages required for trapping are generated by a low-noise, low-drift multichannel arbitrary waveform generator [21]. Exchangeable filter boards close to the trap low-pass the dc electrodes with a cutoff frequency of 10.2 kHz. The trap is operated with radial trap frequencies of about 1.1 MHz and an axial trap frequency of approximately 200 kHz.

Lasers for photoionization, Doppler cooling, and to prevent optical pumping to metastable states are generated using home-built external-cavity diode lasers, referenced to pressure-tight, temperature-stabilized Fabry-Perot cavities resulting in a drift on the order of a few megahertz per day. The wavelengths are measured to a relative level of 10^{-8} using a home-built scanning Michelson interferometer [22] which is compensated for environmental effects such as temperature and pressure changes. A few extensions to the laser system described in [20] were required to match the need for trapping $^{171}Yb^{+}$ ions with its hyperfine splitting: The cooling laser near 369 nm can be shifted using an acousto-optical modulator (AOM) operating at 1.05 GHz in double-pass configuration to resonantly pump ions into the $|S_{1/2}, F = 0\rangle$ hyperfine state as detailed in Sec. IV B. Optical pumping to the $|D_{3/2}, F = 2\rangle$ state is

counteracted by modulating the laser near 935 nm with a fiber electro-optical modulator operating at 3.07 GHz.

The microwave system is similar to the one described in [23]. A notable difference is the usage of a single sideband mixer, which allows destructive interference of the undesired sideband, thus enhancing the power in the desired sideband by a factor of 2. This requires two signals with a frequency-dependent phase and amplitude relation and the setup is thus as follows: Two rf signals provided by two generators are amplified to the desired level and mixed with a local oscillator operating at 12.568 GHz using a single-sideband mixer. The phases and amplitudes of the signal generators are optimized to suppress the unwanted lower sideband, which can be reduced compared to the upper sideband by almost 60 dB [24]. All signal sources are stabilized to a 10 MHz output from a rubidium reference. Synchronous operation of the frequency generators with a defined phase relation is essential, and a dedicated circuitry ensures that trigger events do not occur within a time window around the rising or falling edge of the internal clock of the signal generators, which could result in an unpredictable delay on the order of 5 ns [25,26]. The mixed signal is amplified and applied to the atoms using a horn antenna connected through a low-loss coaxial cable. The microwave system is described in detail in [24].

Fluorescence light from the ion is collected using light-gathering optics with high numerical aperture and a wide field of view [20] and is imaged onto an electron-multiplying charge-coupled device (EMCCD) camera.

B. Experimental sequence

We load $^{171}\mathrm{Yb}^{+}$ ions by resonant isotope-selective ionization of neutral atoms generated in a resistively heated oven [26]. We apply Doppler cooling on the $|S_{1/2},F=1\rangle \leftrightarrow |P_{1/2},F=0\rangle$ transition and counteract optical pumping into the $|S_{1/2},F=0\rangle$ state via off-resonant excitation of the $|P_{1/2},F=1\rangle$ state by applying resonant microwave radiation on the transition $|S_{1/2},F=0\rangle \leftrightarrow |S_{1/2},F=1,m_F=-1\rangle$ (see Fig. 7).

We encode our qubit into the states $|0\rangle \widehat{=} |S_{1/2},F=0\rangle$ and $|1\rangle \widehat{=} |S_{1/2},F=1,m_F=-1\rangle$. Permanent magnets attached to optical mounts for precise alignment create a magnetic field along the weak trap axis of a few gauss which defines the quantization axis and sets the resonance frequency of the σ_- transition used for qubit manipulation. For initial state preparation, the microwave field is switched off, and the cooling laser is blueshifted by 2.1 GHz. This resonantly excites the $|P_{1/2},F=1\rangle$ state and after scattering a few photons, the ion is optically pumped to the $|0\rangle$ state.

As a first step, we roughly estimate the resonance frequency of the σ_- transition by coherent microwave spectroscopy: After preparation of state $|0\rangle$, a microwave pulse of fixed duration is applied, before we project the ion onto state $|0\rangle$ or $|1\rangle$ by scattering resonance fluorescence, and, upon repeating this sequence, determine the excitation probability (or rather the relative frequency of bright and dark events). The dependence of the excitation probability on the frequency of the radiation applied yields an estimate for the resonance frequency and the Rabi frequency. With these estimates, we carry out Ramsey spectroscopy as described in Sec. II for an accurate determination of the resonance frequency.

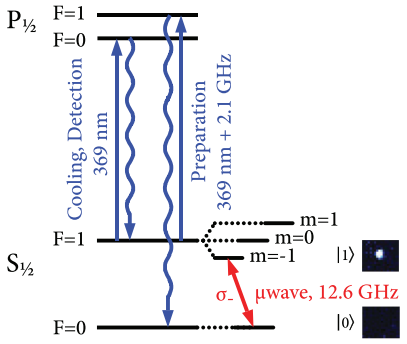

FIG. 7. (Color online) Relevant levels and transitions for laser cooling and qubit preparation, manipulation, and readout of a $^{171}\mathrm{Yb}^{+}$ ion. Doppler cooling is applied on the $|S_{1/2},F=1\rangle \leftrightarrow |P_{1/2},F=0\rangle$ transition. An additional microwave field near 12.6 GHz prevents optical pumping to the $|S_{1/2},F=0\rangle$ state via off-resonant excitation of the $|P_{1/2},F=1\rangle$ state. For preparation, the cooling laser is shifted by 2.1 GHz with an AOM to resonantly pump the ion to the $|S_{1/2},F=0\rangle$ state and the microwave is switched off. Coherent manipulation can now be carried out with the microwave field near 12.6 GHz, which can be tuned by choice to a magnetic-field-sensitive or insensitive transition. Finally, the state is read out by detecting resonance fluorescence from the ion excited by the cooling laser with the microwave field switched off. Additional lasers counteracting optical pumping to metastable states are omitted for clarity.

Flopping of the excitation probability with frequency Δ is observed in a Ramsey experiment, if the driving field is detuned from resonance by Δ, and from such measurements, the resonance can be determined on a hertz level. From a sequence of Ramsey measurements, we estimate the jitter of the resonance frequency ν to be below $\sigma_\nu/2\pi \approx 3$ kHz and a slow drift rate of $|\dot{\nu}|/2\pi < 2$ Hz/s. With the knowledge of the resonance frequency, we determine the on-resonance Rabi-frequency to be $\Omega/2\pi \approx 53$ kHz. Fluctuations of the magnetic fields thus have a negligible effect on the generalized Rabi frequency.

Finally, Ramsey spectroscopy is carried out with and without the optional Hahn π pulse in the middle of the free precession for comparison. In the Sec. III, excitation probabilities are plotted which are determined from the final state of a spinor that was subjected to a free precession for a time τ with a detuning Δ. The error in the detuning Δ is randomized within an interval $(-\epsilon_0,\epsilon_0)$. In the experiment, excitation probabilities have to be inferred from repeated measurements, and for good signal-to-noise ratio, each precession time was repeated 100 times.

The time for a single measurement was limited by the data transfer from the EMCCD camera, and the fact that we synchronize the experiment to a line trigger, so that a single cycle takes 20 or 40 ms. This means that (including some overhead for sequence generation and transmission, etc.) the measurement of each data point takes a few seconds and the entire sequence about 3 to 10 min. Within this time, the resonance frequency is subject not only to random changes within an interval determined by ϵ_0, but also to slow drifts of the resonance on the order of 2 Hz/s, so for a single point, this drift can be neglected, but not for the entire sequence.

There are two common sequential arrangements for the recording of data points: In the first case, the whole array of precession times is recorded and this is done repeatedly; as a consequence, the time between two repetitions of each point is long, such that a drift might be non-negligible. The result of data taken this way is an oscillation with a decaying amplitude, as, for large precession times, a variation of the detuning creates large additional phases and averaging over these phases reduces the contrast. The second option which we used for the measurements presented in this article is to measure each precession time repeatedly, and then to proceed to the next precession time. In this case, drifts for a single point can be neglected. But the points recorded at the end of the sequence might have significantly different detunings compared to the points at the beginning of the sequence. If the data points are taken in order of ascending precession time, the consequence can be an acceleration or deceleration of the fringe frequency. To avoid this effect, we randomized the order in which the precession times were recorded. Therefore, the drifts affect each point as an uncorrelated change of the detuning in a given interval and this allows for a direct comparison with data obtained from theory.

C. Data analysis

Fluorescence from Doppler cooling and state detection is collected on the EMCCD chip and summed over a region of interest. Cycles with low cooling fluorescence are excluded from further consideration. The expected photon distribution from state detection of a dark or bright ion is given by a Poissonian with a mean photon number depending on the qubit state. For ideal repeated measurements of a superposition state, the sum of two Poissonian distributions would be obtained with clearly distinguishable mean photon numbers, and an optimum threshold could be found to decide whether a single shot originates from the projection to a dark or bright ion. In general the detection fidelity suffers from overlapping distributions; in addition, due to the probabilistic amplification process within the gain register of the EMCCD camera the distributions deviate from being Poissonian and the overlap might be increased, but several techniques can further improve statistical significance [27–30]. In the evaluation presented here, ambiguous events were discarded by postselection: we use two threshold values (as discussed in [30] with a primary focus on photomultiplier data), and consider an event dark only if the photon number is below the lower threshold and bright only if the photon number is above the higher threshold. Events with photon numbers between the two thresholds are not considered. The threshold values are found by analyzing photon counting distributions for ions prepared in dark and bright states: the two thresholds are chosen such that the disregarded percentages from the dark distribution and bright distribution are identical. The disregarded percentage can be chosen freely at the expense of more experimental runs or a lower signal-to-noise ratio. By disregarding approximately 20% of the data, as shown in Fig. 8, the fringe contrast improves from 0.948(15) to 0.990(−15, + 10) for the Hahn-Ramsey spectroscopy presented here [shown in Fig. 9(a), lower figure]. Thus, the detection infidelity is reduced by approximately a factor of 5.

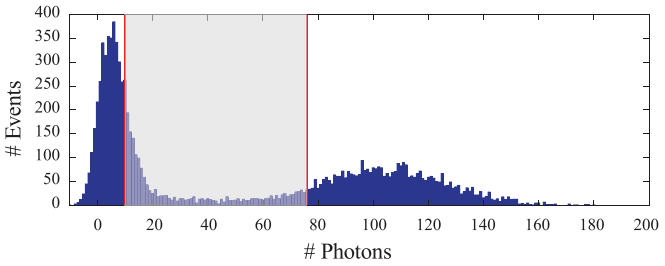

FIG. 8. (Color online) Histogram of the count distribution for detection after Hahn-Ramsey spectroscopy. The gray shaded area between the two thresholds (red vertical lines) indicates the discarded events.

V. EXPERIMENTAL RESULTS

Assigning ϵ_0 in the spirit of Fig. 5 is not strictly possible, as the resonance frequency is not truly random within some interval, but is the consequence of an extended noise spectrum of the magnetic field containing both slow and fast contributions. While noise components in the kilohertz range average even for a single record and reduce the observable contrast, frequency components of a few hertz randomize the resonance of each data point which closely resembles the usage of ϵ in the theory Sec. III, and the drift rate and the time for data taking would yield an ϵ_0 on the order of 1 kHz. Even slower components in the millihertz range can be viewed as drifts, and as their phases are random, the drift rate changes

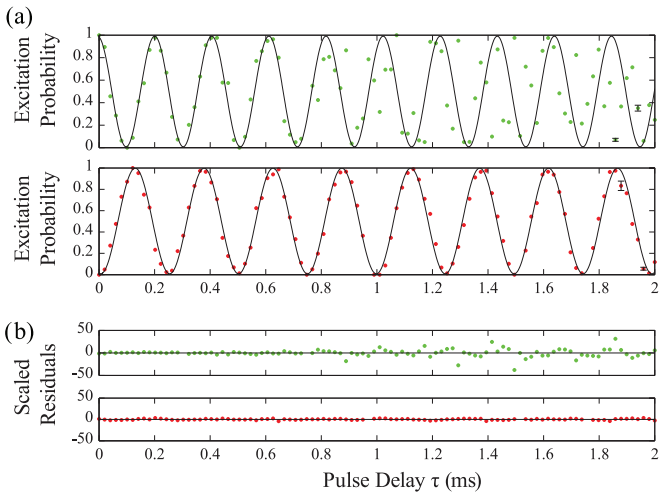

FIG. 9. (Color online) (a) Comparison of standard Ramsey spectroscopy (upper graph) with Hahn-Ramsey spectroscopy (lower graph). All data was taken with the parameters $\Omega/2\pi = 53.46(10)$ kHz, $\Delta = 4$ kHz, and 100 repetitions. Projection errors differ from point to point, and two example error bars are indicated for points with large and small variance, respectively. (b) Scaled deviations $[y_i - f(\vec{p},t_i)]/\sigma_i$ from a sinusoidal least-squares fit $f(\vec{p},t_i)$ to the data with the set of fitting parameters $\vec{p}$, the standard errors σ_i calculated from projection errors, and the time t. The residuals for the standard Ramsey sequence grow beyond $\pm 30\sigma$ and the measured data points become uncorrelated with a sinusoidal curve for large precession times, whereas the residuals for the Hahn-Ramsey sequence in contrast remain roughly within a $\pm 3\sigma$ interval and the data remain nicely sinusoidal for the measured interval.

unpredictably. When a standard Ramsey sequence is applied, single data points at long precession times (>1 ms) can be seemingly uncorrelated to the mean oscillatory behavior, in contrast to the Hahn-Ramsey sequence, where the oscillation remains clean.

The results are shown in Fig. 9 where we compare results of standard Ramsey spectroscopy and Hahn-Ramsey spectroscopy using a pulse sequence as shown in Fig. 1. The improvement using the Hahn-Ramsey approach is clearly visible. For the parameters used here, we could not observe a difference between a usual Hahn π pulse as shown in Fig. 1 and the composite Hahn π pulse as discussed in Fig. 6. The reason for this is the large ratio between Rabi frequency and detuning. If the Rabi frequency is intentionally reduced (or is low because of experimental constraints), the difference is expected to be more significant. To investigate this, we recorded again Hahn-Ramsey signals with a detuning $\Delta = 3.5$ kHz and a reduced Rabi frequency of $\Omega/2\pi = 10.5$ kHz. From Fig. 6 it can be seen that the improvement is pronounced for longer precession times. In addition, we aimed for good signal-to-noise ratio to clearly see the effect, averaging every point over 1000 repetitions. The results are shown in Fig. 10 and the improvement due to the composite π pulse can clearly be seen. In contrast to Fig. 9, the improvement does not appear as a better correlation with a sinusoidal oscillation but as an improvement in fringe contrast. The reason is the large number of repetitions per data point needed to achieve the desired signal-to-noise ratio: as the time required to record a single data point is ten times longer, the assumption that the detuning is constant during that record is no longer fulfilled and the drifts in the experiment reduce the possible contrast for each point. With the composite π pulse, Hahn-Ramsey spectroscopy becomes less susceptible to detuning errors and a larger fringe contrast is recovered.

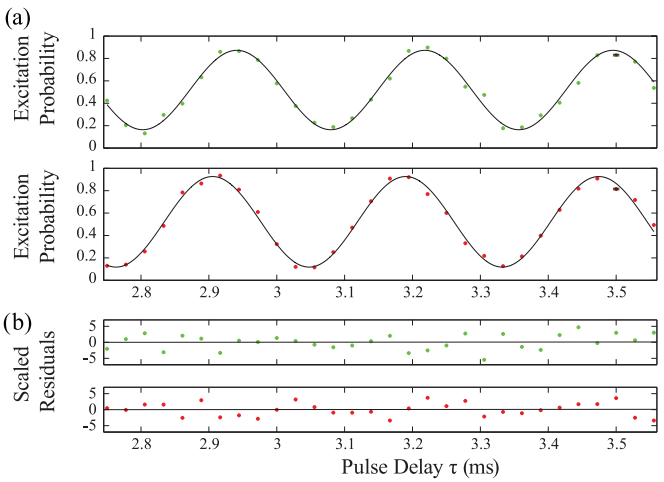

FIG. 10. (Color online) (a) Comparison of a nonrobust (upper graph) and a robust (lower graph) refocusing pulse in Hahn-Ramsey spectroscopy with precession times ranging from 2.75 to 3.55 ms. The effect of robust pulses can be observed best for longer precession times where decoherence already sets in and reduces the visible fringe contrast. As the difference even for those cases is not very pronounced, we aimed for a high signal-to-noise ratio to pinpoint the difference and used 1000 repetitions. The modulation depth for the composite π pulse is 0.808(13) and substantially higher than 0.709(15) obtained for the simple Hahn π pulse. (b) Scaled deviations $[y_i - f(\vec{p},t_i)]/\sigma_i$ from a sinusoidal least-squares fit $f(\vec{p},t_i)$ to the data with the set of fitting parameters $\vec{p}$, the standard errors σ_i calculated from projection and detection errors, and the time t. The mean quadratic scaled deviation for the simple Hahn π pulse is $5.5\sigma^2$ and about 30% larger than the value for the composite Hahn π pulse which is $4.3\sigma^2$.

In conclusion, we could verify the advantages of the detuned π pulse and the robust version of the π pulse experimentally. As expected, the method works best, if the frequency jitter is small compared to the detuning and the detuning is small compared to the Rabi frequency.

VI. DISCUSSION

It is interesting to compare the Hahn-Ramsey technique described and demonstrated here with other modifications of the original two-pulse Ramsey technique. The present scheme bears some similarities to the Ramsey-Bordé schemes [31,32], also known as split-pulse Ramsey sequences, which are widely used for compensation of the linear Doppler shift δ in atomic ensembles. Comparison of the four-pulse and three-pulse Ramsey-Bordé sequences with the present Hahn-Ramsey sequence is made in Fig. 11. In the four-pulse Ramsey-Bordé scheme [Fig. 11(a)], four $\pi/2$ pulses are applied pairwise in opposite directions, which eliminates the linear Doppler shift δ. However, the error ϵ due to frequency drifts of the radiation source itself, as discussed here, cannot be canceled because ϵ always adds with the detuning Δ as $\Delta + \epsilon$ and hence it cannot be discriminated from Δ.

Apart from the reversed sign of the detuning of the spin-echo π pulse, the present scheme is similar to the three-pulse Ramsey-Bordé sequence [Fig. 11(b)] wherein no such detuning sign flip is present [8,13]. In the latter, the middle π pulse cancels (to first order) the dependence of the Ramsey fringes on any frequency shifts from resonance. The fringes are observed as a function of the phase shift in one of the Ramsey $\pi/2$ pulses or as a function of the phase shift of one of the qubit states during the free evolution between the pulses. In contrast, in the present fault-tolerant Hahn-Ramsey sequence the preselected detuning Δ and the radiation source error ϵ add up differently, as $\Delta + \epsilon$ and $\Delta - \epsilon$, which makes it possible to cancel the dependence on ϵ while keeping that on Δ. Because the detuning Δ determines the fringe frequency, the fringes can be observed in the original Ramsey manner, by plotting the signal as a function of the separation τ between the pulses or versus the detuning Δ (which is not possible in the three-pulse Ramsey-Bordé scheme). The fringes can be observed also as a function of the relative phase between the pulses. It is important that the fault-tolerant Hahn-Ramsey sequence allows one also to cancel Doppler shifts of moving atoms when applying all three pulses in the same direction, as seen in Fig. 11(c), because the Doppler shift adds up in the same manner as the driving frequency drift ϵ.

Another useful feature of the present Hahn-Ramsey scheme is that it does not assume that the pulse durations are very small, as is customary in the Ramsey scheme and its variations, but only that the Rabi frequency is larger than the detuning. Indeed, the performance of this scheme improves as the pulse durations decrease (and hence the Rabi frequencies increase

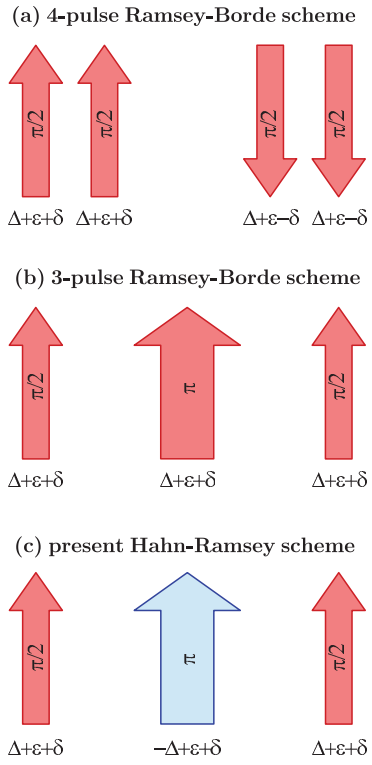

FIG. 11. (Color online) Comparison of (a) the four-pulse and (b) the three-pulse Ramsey-Bordé sequences with (c) the present Hahn-Ramsey sequence. The arrows indicate the spatial direction of each pulse and the expressions beneath them show the total frequency offset from resonance due to the driving field detuning Δ, the driving field frequency drift ϵ, and the Doppler shift δ. The application of the pulses in opposite directions in the four-pulse Ramsey-Bordé scheme eliminates the first-order Doppler shift δ in atomic ensembles, but the frequency drift ϵ cannot be canceled because it adds to the detuning Δ in the same manner and hence it cannot be separated from Δ. In the three-pulse Ramsey-Bordé scheme (b) the drift ϵ is eliminated altogether with the Doppler shift δ and the detuning Δ, and hence no dependence on Δ is left in the signal. In the present Hahn-Ramsey scheme (c) both the drift ϵ and the Doppler shift δ can be canceled if all the pulses are copropagating because they add up differently to the detuning Δ.

in order to maintain the pulse areas at $\pi/2$ or π). However, it works very well even for moderate pulse durations when the Rabi frequency is comparable to (but still larger than) the detuning, especially with the use of a composite middle π pulse, as in Figs. 6 and 10.

An additional π pulse between the two $\pi/2$ Ramsey pulses has been used before for other purposes and in a different manner. Lundblad *et al.* [33] used such a pulse in order to enhance the sensitivity of Ramsey fringes to decoherence. Yudin *et al.* proposed [15], and Huntemann *et al.* demonstrated [10], the use of such a pulse for cancellation of the dynamic Stark shift induced by the driving fields themselves. The additional π pulse was merged with the second $\pi/2$ pulse but had a π phase shift and its frequency was shifted by the anticipated light shift. It was essential that these light shifts were present during the driving pulses only. The fault-tolerant Hahn-Ramsey scheme proposed here allows one to cancel the effect of random drifts in the carrier frequency of the driving pulses from shot to shot. These drifts affect the entire evolution, during as well as between the pulses, and cannot be canceled by the scheme of Refs. [10,15].

Finally, we note that there are other, more sophisticated rephasing sequences than Hahn's spin echo, such as the Carr-Purcell-Meiboom-Gill two-pulse sequence [34,35] and its extensions. However, the very simple single-pulse Hahn's scheme used here appears to be sufficient to compensate the type of random detuning error considered.

VII. CONCLUSION

In this paper, we have examined the sensitivity of the Ramsey technique to random errors ϵ in the detuning of the driving oscillating fields. We have especially focused on the use of the Ramsey technique for detection and characterization of quantum coherence, which is deduced from the Ramsey signal plotted versus the pulse delay. The classical two-pulse Ramsey scheme is very sensitive to such detuning errors because they directly change the frequency of the Ramsey fringes and make the latter decohere. The simple approach of adding two signals of opposite detunings Δ and $-\Delta$ can compensate only very small detuning errors ϵ because the amplitude of the Ramsey fringes undergoes a global sinusoidal modulation at the frequency ϵ. We have proposed here to combine the Ramsey method with ideas from Hahn's spin-echo technique by adding a pulse of double duration $2T$ and opposite detuning $-\Delta$ in the middle between the two Ramsey $\pi/2$ pulses. The resulting Hahn-Ramsey fringes are rephased very accurately even for very large detuning errors ($|\epsilon/\Delta| \lesssim 0.5$) provided the Rabi frequency of the driving fields is sufficiently larger than the detuning ($\Omega \gtrsim 5\Delta$). If it is not possible to have such a large Rabi frequency, then one can replace the middle $2T$ pulse, which for $\Omega/\Delta \lesssim 3$ deviates significantly from a π pulse, by a two-component composite pulse, which acts as a perfect π pulse. These features have been demonstrated experimentally with $^{171}Yb^{+}$ ions trapped in a segmented linear Paul trap, in nearly perfect agreement with the theory.

The proposed Hahn-Ramsey technique should be a useful tool for observation of high-resolution Ramsey fringes even when the driving field undergoes undesired parameter variations during the course of measurement [14]. It makes it also possible to use Ramsey spectroscopy in atomic ensembles with significant inhomogeneous broadening, as in doped solids [36,37]; in this case the detuning Δ should be larger than the inhomogeneous bandwidth for the Hahn-Ramsey scheme to be applicable.

ACKNOWLEDGMENTS

We acknowledge funding from the European Community's Seventh Framework Program (FP7) under Grant Agreement No. 270843 (iQIT) and the European Metrology Research Program (EMRP), which is jointly funded by the EMRP participating countries within EURAMET and the European Union (EU). N.V.V. acknowledges support by the Alexander-von-Humboldt Foundation and stimulating discussions with Thomas Halfmann.

[1] N. F. Ramsey, Phys. Rev. **78**, 695 (1950).
[2] N. F. Ramsey and H. B. Silsbee, Phys. Rev. **84**, 506 (1951).
[3] N. F. Ramsey, Rev. Sci. Instrum. **28**, 57 (1957).
[4] N. F. Ramsey, Phys. Rev. **109**, 822 (1958).
[5] N. F. Ramsey, Phys. Today **33**(7), 25 (1980); **66**(1), 36 (2013).
[6] N. F. Ramsey, Rev. Mod. Phys. **62**, 541 (1990).
[7] V. Giovannetti, S. Lloyd, and L. Maccone, Nat. Photonics **5**, 222 (2011).
[8] M. Riebe, H. Häffner, C. F. Roos, W. Hänsel, J. Benhelm, G. P. T. Lancaster, T. W. Körber, C. Becher, F. Schmidt-Kaler, D. F. V. James, and R. Blatt, Nature (London) **429**, 734 (2004).
[9] N. V. Vitanov and P. L. Knight, Phys. Rev. A **52**, 2245 (1995).
[10] N. Huntemann, B. Lipphardt, M. Okhapkin, Chr. Tamm, E. Peik, A. V. Taichenachev, and V. I. Yudin, Phys. Rev. Lett. **109**, 213002 (2012).
[11] H. Häffner, S. Gulde, M. Riebe, G. Lancaster, C. Becher, J. Eschner, F. Schmidt-Kaler, and R. Blatt, Phys. Rev. Lett. **90**, 143602 (2003).
[12] N. Timoney, I. Baumgart, M. Johanning, A. F. Varon, M. B. Plenio, A. Retzker, and C. Wunderlich, Nature (London) **476**, 185 (2011).
[13] S. C. Webster, S. Weidt, K. Lake, J. J. McLoughlin, and W. K. Hensinger, Phys. Rev. Lett. **111**, 140501 (2013).
[14] C. Piltz, B. Scharfenberger, A. Khromova, A. F. Varón, and C. Wunderlich, Phys. Rev. Lett. **110**, 200501 (2013).
[15] V. I. Yudin, A. V. Taichenachev, C. W. Oates, Z. W. Barber, N. D. Lemke, A. D. Ludlow, U. Sterr, C. Lisdat, and F. Riehle, Phys. Rev. A **82**, 011804(R) (2010).
[16] E. L. Hahn, Phys. Rev. **80**, 580 (1950).
[17] B. W. Shore, *The Theory of Coherent Atomic Excitation* (Wiley, New York, 1990).
[18] M. H. Levitt, Prog. Nucl. Magn. Reson. Spectrosc. **18**, 61 (1986).
[19] S. Schulz, U. Poschinger, F. Ziesel, and F. Schmidt-Kaler, New J. Phys. **10**, 045007 (2008).
[20] D. Kaufmann, T. Collath, M. T. Baig, P. Kaufmann, E. Asenwar, M. Johanning, and Chr. Wunderlich, Appl. Phys. B **107**, 935 (2012).
[21] M. T. Baig, M. Johanning, A. Wiese, S. Heidbrink, M. Ziolkowski, and Chr. Wunderlich, Rev. Sci. Instrum. **84**, 124701 (2013).
[22] P. Kaufmann, Diploma thesis, University of Siegen, (2012).
[23] A. Khromova, Ch. Piltz, B. Scharfenberger, T. F. Gloger, M. Johanning, A. F. Varon, and Ch. Wunderlich, Phys. Rev. Lett. **108**, 220502 (2012).
[24] T. F. Gloger, MS thesis, University of Siegen, 2011.
[25] C. Weiss, Diploma thesis, University of Siegen, 2007.
[26] M. Johanning, A. Braun, D. Eiteneuer, Chr. Paape, Chr. Balzer, W. Neuhauser, and Chr. Wunderlich, Appl. Phys. B **103**, 327 (2011).
[27] R. Noek, G. Vrijsen, D. Gaultney, E. Mount, T. Kim, P. Maunz, and J. Kim, Opt. Lett **38**, 4735 (2013).
[28] A. H. Myerson, D. J. Szwer, S. C. Webster, D. T. C. Allcock, M. J. Curtis, G. Imreh, J. A. Sherman, D. N. Stacey, A. M. Steane, and D. M. Lucas, Phys. Rev. Lett. **100**, 200502 (2008).
[29] B. Hemmerling, F. Gebert, Y. Wan *et al.*, New J. Phys. **14**, 023043 (2012).
[30] S. Wölk *et al.*, J. Phys. B: At. Mol. Opt. Phys. **48**, 075101 (2015).
[31] C. J. Bordé, C. Salomon, S. Avrillier, A. Van Lerberghe, C. Bréant, D. Bassi, and G. Scoles, Phys. Rev. A **30**, 1836 (1984).
[32] C. J. Bordé, Phys. Lett. A **140**, 10 (1989).
[33] N. Lundblad, J. M. Obrecht, I. B. Spielman, and J. V. Porto, Nat. Phys. **5**, 575 (2009).
[34] H. Y. Carr and E. M. Purcell, Phys. Rev. **94**, 630 (1954).
[35] S. Meiboom and D. Gill, Rev. Sci. Instrum. **29**, 688 (1958).
[36] G. Heinze, C. Hubrich, and T. Halfmann, Phys. Rev. Lett. **111**, 033601 (2013).
[37] G. T. Genov, D. Schraft, T. Halfmann, and N. V. Vitanov, Phys. Rev. Lett. **113**, 043001 (2014).